Infiltration of Macromolecules into Nanoporous Silica Particles

Yajun Wang, Alexandra S. Angelatos, Dave E. Dunstan, and Frank Caruso*

Centre for Nanoscience and Nanotechnology, Department of Chemical and Biomolecular Engineering, The University of Melbourne, Victoria 3010, Australia

Received May 18, 2007; Revised Manuscript Received July 30, 2007

ABSTRACT: The immobilization of macromolecules within porous materials for applications such as biosensing, biocatalysis, drug delivery, and protein separation requires an understanding of the conditions under which nanopores are accessible to macromolecules. We report the results of a detailed investigation into the infiltration of a polymer probe, poly(acrylic acid) (PAA) of different molecular weights (2000−250 000 g mol^{-1}), in amine-functionalized nanoporous silica particles with a series of pore sizes (4−40 nm). The surface charge of the nanopores and the charge density and conformation of PAA were tuned by changing the PAA solution conditions (e.g., pH and ionic strength) to which the particles were exposed. Thermogravimetric analysis and dynamic light scattering revealed that the extent of PAA infiltration strongly depends upon the relative sizes of the nanopores and the PAA molecules—the larger the nanopores, the broader the range of PAA molecular weights that can infiltrate the particles. These techniques also revealed that as the pH of the PAA solution increased above 3, the amount of PAA loaded in the particles decreased due to the polymer chains adopting a more extended conformation. In addition, it was found that the ionic strength of the PAA solution played a relatively complex role in PAA infiltration, as electrolytes can screen both the polyelectrolyte charge and the particle surface charge. Loading of PAA in the nanopores was confirmed by transmission electron microscopy of the replicated nanoporous polymer materials, which were prepared by cross-linking the infiltrated polymer and removing the silica template particles. The distribution of PAA in the nanoporous silica particles was examined by confocal laser scanning microscopy after binding fluorescent doxorubicin to the loaded PAA via electrostatic association.

Introduction

The discovery of mesoporous silicas (MSs), materials with pore diameters between 2 and 50 nm, has created new possibilities in many areas of chemistry and materials science.[1] Because of their high specific surface areas and pore volumes, and their well-ordered uniform pore structures, MSs are attractive supports for the adsorption of macromolecules (e.g., enzymes).[2] MSs are also widely used as templates to fabricate a variety of materials, including metal,[3] metal oxide,[4] carbon,[5] and polymer[6] replicas. We recently reported the preparation of nanoporous polymer spheres (NPSs) via the sequential assembly of macromolecules (e.g., polyelectrolytes, peptides, and proteins) in MS particles, followed by removal of the particle templates.[7] The application of MSs as supports for adsorption or as templates for the synthesis of polymer replicas relies upon the infiltration of macromolecules in the nanopores. Thus, to exploit the potential of macromolecule-functionalized MSs in areas such as biosensing,[8] biocatalysis,[9] drug delivery,[10] and protein separation,[11] it is essential to understand the various conditions under which macromolecules can access the nanopores of MSs.[12]

A number of theoretical models based on reptation dynamics[13] have been proposed to understand the diffusion of charged linear polymers through random fixed obstacles, as in gel electrophoresis of DNA molecules[14] and the release of double-stranded DNA from the bacteriophage.[15] The key assumption underlying these reptation models is that the entangled chain is confined, due to topological constraints imposed by the surrounding chains, to diffuse primarily along a path that follows its own contour.[16] While this concept of the tube-like motion of a polyelectrolyte through a confined space may aid in the understanding of how macromolecules infiltrate MSs, to the best of our knowledge, there has not yet been a study that systematically investigates the influence of key parameters (e.g., macromolecule size, pore size, pH, and ionic strength) on macromolecule infiltration in nanoporous particles.

Herein, we report the use of poly(acrylic acid) (PAA) to probe macromolecule infiltration in nanopores. A key advantage of this synthetic polymer is that it is available in a range of different sizes, which allows for determination of the relationship between macromolecule size and degree of loading. In addition, PAA is a weak polyelectrolyte that is highly stable under a range of solution conditions, and so by adjusting the solution pH and ionic strength, the effect of charge density and conformation of the macromolecules can be studied.[17] The influence of nanopore size on PAA infiltration is examined by using several amine-functionalized MSs with a series of pore sizes (4−40 nm).

Experimental Procedures

Materials. PAA of different weight-average molecular weights (2000, 8000, 30 000, 100 000, and 250 000 g mol^{-1}, denoted hereafter as PAA-2k, PAA-8k, PAA-30k, PAA-100k, and PAA-250k, respectively) in the acid form (PAA-2k, PAA-100k, and PAA-250k) and in the sodium salt form (PAA-8k and PAA-30k), (ethylene oxide)$_{20}$-*b*-(propylene oxide)$_{70}$-*b*-(ethylene oxide)$_{20}$ block copolymer (P_{123}, 5800 g mol^{-1}), cetyltrimethylammonium bromide (CTABr), 3-aminopropyl-triethoxysilane (APTS), *n*-dodecylamine, decane, ethyl acetate, ethanol, toluene, methanol, hydrochloric acid (HCl), sodium hydroxide (NaOH), sodium chloride (NaCl), sodium metasilicate (Na_2SiO_3), tetraethyl orthosilicate (TEOS, 98%), ammonia solution (25 wt % in water), ethylenediamine, 1-ethyl-3-(3-dimethylaminopropyl) carbodiimide hydrochloride (EDC), doxorubicin (DOX), hydrofluoric acid (HF), and 2-propanol were obtained from Sigma-Aldrich and used as received. The water used in all experiments was prepared in a Millipore Milli-Q purification system and had a resistivity higher than 18 MΩ cm.

Nanoporous Particles. MS particles with ordered pores (4.0, 5.9, and 10.6 nm) and bimodal pores (2−3 nm (av 2.7 nm) and

* Corresponding author. E-mail: fcaruso@unimelb.edu.au.

10.1021/ma071125s CCC: $37.00
Published on Web 09/20/2007

Table 1. Properties of MS Particles Used for PAA Infiltration

particles	particle morphology	pore structure	av pore size[a] (nm)	pore volume ($cm^3\ g^{-1}$)	surface area[b] ($m^2\ g^{-1}$)
S_4	nonuniform	ordered	4.0	0.28	259
S_6	nonuniform	ordered	5.9	0.67	448
S_{11}	nonuniform	ordered	10.6	0.83	284
$S_{3,28}$	spherical	bimodal	2.7, 28.3[c]	1.35	465

[a] Calculated by the Barrett−Joyner−Halender (BJH) method from the adsorption branch. [b] Calculated by the BET method. [c] On the basis of smaller mesopores and larger mesopores.

10−40 nm (av 28.3 nm)) were used. These particles are denoted as S_4, S_6, S_{11}, and $S_{3,28}$, respectively, according to their pore diameters (see Table 1 for properties of these nanoporous particles). The S_4 and S_6 particles were prepared by dissolving 2 g of P_{123} in 15 mL of Milli-Q water at 30 °C, after which 30 g of a 2 M HCl solution was added, followed by 4.4 g of TEOS (drop-wise addition).[18] The mixture was stirred at 30 °C for 24 h, after which it was transferred to a sealed Teflon bottle in an autoclave. The samples were then heated to 60 °C (for sample S_4) or 100 °C (for sample S_6) for 48 h in an oven. The S_{11} particles were prepared by dissolving 2.4 g of P_{123} and 14 g of decane in 84 mL of HCl solution (1.07 M).[19] After stirring the mixture at room temperature for 2 h, 0.027 g of ammonium fluoride was added, followed by 5.1 g of TEOS under stirring. The previous mixture was stirred at 40 °C for 20 h and then transferred to an autoclave for further reaction at 100 °C for 48 h. The $S_{3,28}$ particles were prepared by dissolving 9.8 g of CTABr and 5 g of Na_2SiO_3 to form a clear solution in 175 mL of Milli-Q water in a polyethylene bottle at 30 °C. A total of 17.5 mL of ethyl acetate was then added.[20] The mixture was stirred for 30 s and allowed to stand at ambient temperature (20 °C) for 5 h. After this period of aging, the bottle was maintained at 90 °C for 48 h in an oil bath.

The as-synthesized particles were collected by centrifugation and then washed 3 times with ethanol and twice with Milli-Q water. After air drying at room temperature, the particles were calcined at 500 °C for 5 h to remove the surfactants. The porous silica particles were then functionalized with a layer of primary amine groups by APTS grafting. In this process, the calcined particles were dispersed in toluene by sonication for 20 min before APTS was added to the suspension.[21] The molar ratio of the MS particles (calculated as SiO_2/APTS/toluene) was fixed at 5:1:500, and the suspension was refluxed for 24 h. The APTS-grafted particles were collected by centrifugation and then washed once with toluene and twice with methanol. Finally, the pellet was dried at 80 °C for 12 h. The degree of functionalization (estimated via thermogravimetric analysis (TGA)) was ca. 1.9 amine groups per nm^2 of silica, both on the outer particle surface and within the nanopores.[21]

Macromolecule Infiltration. PAA solutions with a concentration of 5 mg mL^{-1} were used. The solutions were prepared by dissolving PAA in deionized water and adjusting the solution pH with 0.1 M HCl or NaOH. The ionic strength (NaCl concentration) of the solutions ranged from 0.05 to 1 M. The infiltration experiments typically involved mixing 2 mL of PAA solution with 10 mg of MS powder (PAA/silica weight ratio of 1:1) and then shaking the mixture at room temperature for 24 h. After separating the PAA supernatant from the particles by centrifugation, the particles were washed twice with Milli-Q water, and then the pellets were dried at room temperature. The washing process was completed in ca. 2 min—longer washing times do not alter the degree of macromolecule infiltration (data not shown). The PAA loading (i.e., the amount of PAA infiltrated into the particles) was determined by TGA, and then the specific PAA loading was calculated based on the surface area of the particles.[22]

Instrumentation. The surface areas and porosities of the MS particles were measured by a Micromeritics Tristar surface area and porosity analyzer at −196 °C using nitrogen as the adsorption gas. TGA experiments were conducted on a Mettler Toledo/TGA/SDTA851e Module analyzer. The samples were heated from 25 to 120 °C with a heating rate of 5 °C per min and kept at 120 °C for 20 min under nitrogen (30 mL min^{-1}). They were then heated from 120 to 550 °C with a heating rate of 10 °C per min under oxygen (30 mL min^{-1}). DLS measurements were performed on 5 mg mL^{-1} PAA solutions using a Malvern 4700 apparatus with a 10 mW argon ion laser at 488 nm. Analysis was carried out at an angle of 90° and a temperature of 25 °C. The time auto-correlation functions were analyzed using an inverse Laplace transform algorithm (CONTIN) to obtain a distribution of relaxation times related to the diffusion coefficient (*D*). The *D* values were converted to radii using the Stokes−Einstein equation and a solvent (water) viscosity of 0.89 mPa s. The errors associated with the radii values were estimated from the widths of the size distributions obtained. Zeta potentials were measured using a Malvern 2000 Zetasizer. The influence of pH on particle charge was examined in aqueous solutions with no added electrolyte, while the effect of ionic strength on particle charge was investigated in NaCl solutions (0−1 M) at pH 4.5. Transmission electron microscopy (TEM, Philips CM120 BioTWIN, operated at 120 kV) and scanning electron microscopy (SEM, FEI Quanta 200 FEG, operated at 10 kV) were used to examine the particle morphologies. The TEM samples (2 μL) were placed onto Formvar-coated copper grids and allowed to air-dry. The SEM samples (20 μL) were placed onto silicon wafers and allowed to air-dry prior to gold sputter-coating. Confocal laser scanning microscopy (CLSM) images were taken with a Leica DMIRE2 confocal system. The samples (2 μL) were placed onto glass slides and viewed using a 60× oil immersion objective.

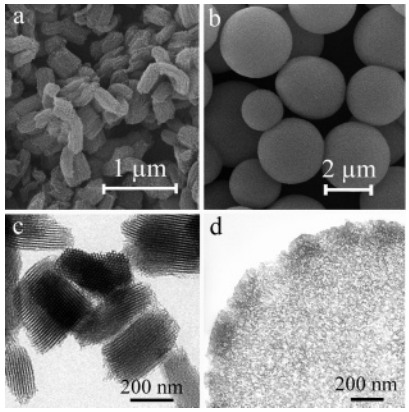

Figure 1. SEM images of (a) S_{11} particles and (b) $S_{3,28}$ particles. TEM images of (c) S_{11} particles and (d) an ultramicrotomed sample (ca. 90 nm thin slice) of a $S_{3,28}$ particle.

Results and Discussion

Nanoporous Particles. MS particles with a series of pore sizes were used to study the effect of pore size on PAA infiltration. Before use, the particles were functionalized with a layer of amine groups by grafting APTS to the surface of the pore walls, thereby rendering the particles positively charged with a stable charge density.[21] The properties of the APTS-modified particles are summarized in Table 1. The S_4, S_6, and S_{11} particles are nonuniform in morphology but possess a hexagonal arrangement of uniform mesopores, and so these particles were selected as the nanoporous particles to study the parameters that influence PAA infiltration. Figure 1a,c shows SEM and TEM images, respectively, of the S_{11} particles, which are also representative of the S_4 and S_6 particles. In contrast, the $S_{3,28}$ particles (Figure 1b,d) are uniform in morphology (i.e., spheres with a diameter of ca. 2−3 μm) but possess a bimodal pore structure (i.e., 2−3 and 10−40 nm pores). The $S_{3,28}$ particles were used for comparison with the S_4, S_6, and S_{11} particles. Recently, we have used such bimodal MS particles for the encapsulation of macromolecules[23] and for the template synthesis of polymer-based materials.[7]

PAA Infiltration. To establish the optimum values for the adsorption time and the PAA/silica mass ratio, S_6 particles were

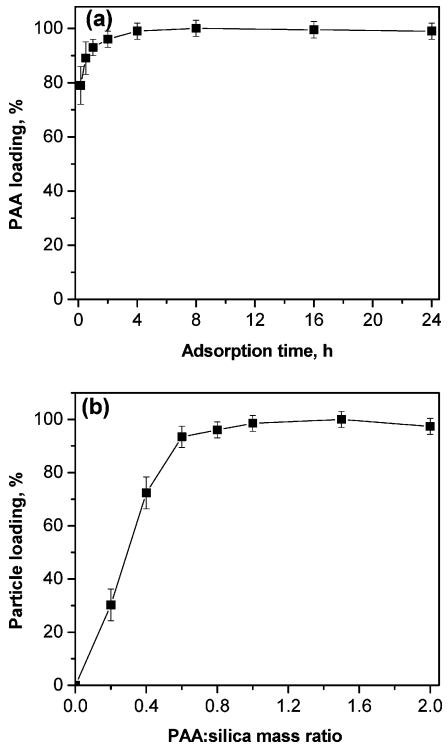

Figure 2. (a) Loading of PAA-30k in S_6 particles vs adsorption time (PAA/silica mass ratio, 1; pH, 4.5; and NaCl concentration, 0.5 M). (b) Loading of S_6 particles with PAA-30k vs PAA/silica mass ratio (adsorption time, 24 h; pH, 4.5; and NaCl concentration, 0.5 M).

incubated with PAA-30k at pH 4.5 in 0.5 M NaCl. The S_6 particles were selected for these preliminary experiments as they are the mid-size MS particles with ordered pores used in this study. Similarly, PAA-30k was employed as it represents the mid-size polymer in the range of PAA molecular weights studied. The pH and NaCl concentration were set at 4.5 and 0.5 M, respectively, because previous experiments have shown that significant PAA infiltration occurs under similar solution conditions.[7b,c]

Figure 2 depicts the variation in the PAA loading with adsorption time (Figure 2a) and the particle loading with PAA/silica mass ratio (Figure 2b). The data show that, for a fixed PAA/silica mass ratio of 1, PAA adsorption reaches saturation after 4 h, with 80% of saturation loading being attained within the first 10 min. The data also show that, for a fixed adsorption time of 24 h, the particle loading increases significantly as the PAA/silica mass ratio is increased from 0 to 0.6, reaching saturation at a PAA/silica mass ratio of about 0.8. Thus, an adsorption time of 24 h and a PAA/silica mass ratio of 1 result in saturation loading of PAA-30k in the S_6 particles at pH 4.5 in 0.5 M NaCl. The same adsorption time (24 h) and PAA/silica mass ratio (1) were employed for all subsequent experiments to facilitate comparisons between the different systems.

Influence of PAA Molecular Weight and Pore Size. To study the influence of PAA size on the degree of PAA infiltration, PAA solutions with different molecular weights were used. The variation in the hydrodynamic radius (R_h) of PAA with molecular weight is shown in Figure 3a. The DLS measurements were performed using the same solution conditions as in the infiltration experiments (i.e., pH 4.5 and 0.5 M NaCl). As the PAA molecular weight increases, the polymer chain length, and hence R_h, increases. However, the rate of increase in R_h with molecular weight gradually decreases for the larger PAA molecules (>100 000 g mol^{-1}). The largest PAA used in this study (250 000 g mol^{-1}) has a diameter of 11.4 ± 2.0 nm (i.e., an R_h of 5.7 ± 1.0 nm), which is similar to the diameter of the pores for the S_{11} particles (10.6 nm). The influence of pore size was investigated by infiltrating the various PAA molecules in a series of well-ordered nanopores ranging from 4 to 11 nm (i.e., the S_4, S_6, and S_{11} particles). As Figure 3b shows, for each of the PAA molecular weights used, the PAA loading increases with pore size, indicating that the larger nanopores are more accessible to the macromolecules. This increase in the PAA loading with pore size becomes more pronounced as the PAA molecular weight increases; the larger the macromolecule, the greater the influence of pore size on loading. For example, the pore size has a negligible effect on the PAA-2k loading beyond 6 nm. The diameter of PAA-2k (2.0 ± 0.8 nm) is well below the pore diameter for the S_6 particles (5.9 nm) and the S_{11} particles (10.6 nm); hence, PAA-2k can infiltrate these nanoporous particles to effectively the same extent. In contrast, the loading increases almost linearly with pore size for the larger PAA molecules. For example, the amount of PAA-2k loaded in the S_{11} particles is only ca. 1.5 times higher than that for the S_4 particles, as compared to a factor of ca. 5.3 in the case of PAA-250k.

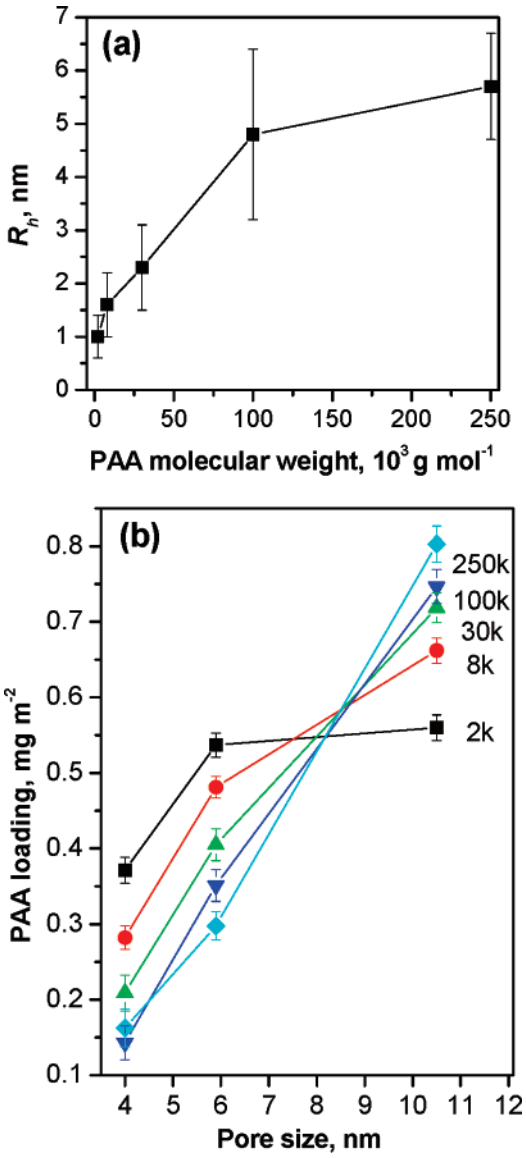

Figure 3. (a) Influence of PAA molecular weight on PAA R_h (pH, 4.5 and NaCl concentration, 0.5 M). (b) Influence of pore size on PAA loading for the various PAA molecular weights (adsorption time, 24 h; PAA/silica mass ratio, 1; pH, 4.5; and NaCl concentration, 0.5 M).

The $S_{3,28}$ particles were also examined for comparison. Although the average pore size for the $S_{3,28}$ particles (12.7 nm) is greater than that for the S_{11} particles (10.6 nm), the S_{11} particles exhibit a higher PAA loading ability than the $S_{3,28}$ particles (see later). This may be attributed to the coexistence of large pores (10−40 nm) and small pores (2−3 nm) within the $S_{3,28}$ particles because, while the small pores make a significant contribution to the total particle surface area (ca. 20%), they are not effective for PAA loading. In addition, it is likely that the random arrangement of nanopores within the $S_{3,28}$ particles (as opposed to the ordered hexagonal arrangement of nanopores within the S_{11} particles) creates a more tortuous path, thus restricting PAA infiltration.

Influence of pH. PAA is a weak polyelectrolyte (the pK_a of PAA in solution in the absence of added salt ranges from ca. 5.5 to 6.5),[24] and so the ionization (and hence conformation) of the polymer depends upon the pH. Under alkaline conditions, PAA has a high charge density, resulting in an extended conformation, whereas under acidic conditions (pH ca. 2−6), PAA has a low charge density, leading to a coiled conformation.[25] Under extreme acidic conditions (pH < 2), most of the carboxylic acid groups along the PAA chain are protonated.

The effect of pH on the surface charge of the APTS-modified MS particles was investigated using the S_{11} particles. As Figure 4a illustrates, the particles possess a high charge (>25 mV) over a wide pH range (ca. 1−7). This indicates that the influence of pH on PAA infiltration may be studied over this range without inducing significant changes in the particle charge.

To examine the effect of pH on PAA infiltration, the pH of the PAA solutions (containing 0.5 M NaCl) was varied. The loading of PAA-30k in the various nanoporous particles decreases as the pH increases (Figure 4b). A likely explanation is that as the pH increases, the PAA charge density increases, and the polymer chains adopt a more extended, rigid conformation to minimize intramolecular electrostatic repulsions, resulting in the macromolecules being spatially excluded from the nanopores (Figure 5). This explanation is supported by the DLS experiments. For example, the R_h of PAA-250k increases from 5.7 ± 1.0 to 7.6 ± 2.0 nm when the solution pH is changed from 4.5 to 8 in 0.5 M NaCl (DLS data not shown). However, at a lower pH of 3.5, the R_h of PAA-250k appears to be relatively large (8.2 ± 2.0 nm). This may be attributed to the polymer molecules tending to cluster in solution when the charge density along the polymer chains, and hence the intermolecular electrostatic repulsion, is reduced.[26] A decrease in the electrostatic repulsions among the species to be loaded permits a denser packing, and hence a higher loading, within the nanoporous silica materials. This finding is supported by the work of Vinu et al.,[12b] who studied the adsorption of cytochrome *c* onto various mesoporous molecular sieves at different solution pHs. They found that adsorption is maximal at pH 9.6, which is close to the isoelectric point of cytochrome *c* (9.8) because the net charge of the protein is low, and hence, the repulsive force between the protein molecules is minimal, permitting a closer packing of the protein molecules.

Influence of Ionic Strength. Polyelectrolyte multilayer films are typically thicker when assembled in the presence of salt.[27] This is due to the salt ions partially screening the charges on the polyelectrolytes, thereby reducing both intra- and intermolecular electrostatic repulsions and causing the macromolecules to adopt a more coiled, compact conformation.[28] Salt can also partially screen the charges on the surface of the APTS-modified MS particles (i.e., the positive surface charge on the particles decreases with increasing salt concentration (from ca. 37 mV at 0 M NaCl to ca. 8 mV at 1 M NaCl; zeta potential data not shown)). Thus, in the presence of salt, the degree of PAA loading in nanoporous particles is governed by a balance between screening of the polyelectrolyte charge (which reduces intra- and intermolecular electrostatic repulsions, thereby promoting infiltration) and screening of the particle surface charge (which reduces the polyelectrolyte−particle electrostatic attraction).

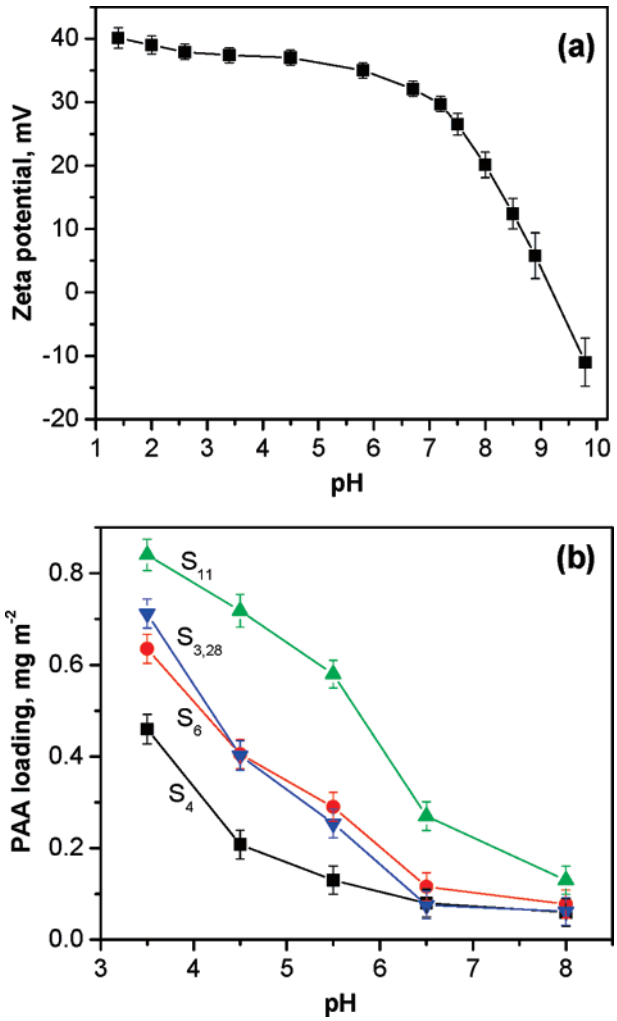

Figure 4. (a) Surface charge of the APTS-modified S_{11} particles vs pH (NaCl concentration, 0 M). (b) Influence of pH on PAA loading in the various nanoporous particles (adsorption time, 24 h; PAA/silica mass ratio, 1; PAA molecular weight, 30 000 g mol^{-1}; and NaCl concentration, 0.5 M).

To investigate the effect of ionic strength on PAA infiltration in the S_{11} particles, the NaCl concentration of the PAA solutions (at pH 4.5) was varied from 0.05 to 1 M. As shown in Figure 6, the PAA loading decreases linearly with increasing salt concentration for PAA molecules below 100 000 g mol^{-1}. Further, the lower the PAA molecular weight, the sharper the decrease. This reduction in PAA loading with increasing ionic strength is attributed to increased screening of the particle surface charge by salt ions, which weakens the electrostatic attraction between the PAA molecules and the nanopores,[29] outweighing the benefit of the reduced PAA molecular size with increasing salt concentration.

In the case of PAA-250k, a different trend is observed. The loading increases significantly from 0.14 to 0.78 mg m^{-2} as the salt concentration is increased from 0.05 to 0.5 M, after which the loading plateaus and then decreases with further increases in the salt concentration (Figure 6). This result may

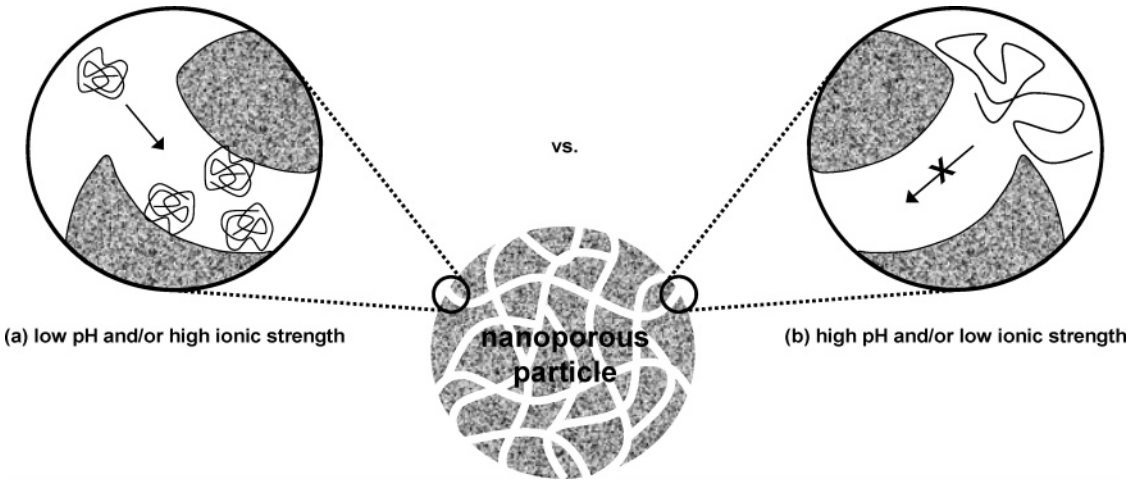

Figure 5. Schematic representation of two extreme cases: (a) low pH and/or high ionic strength (resulting in infiltration of coiled PAA molecules in the nanopores) and (b) high pH and/or low ionic strength (resulting in exclusion of extended PAA molecules from the nanopores).

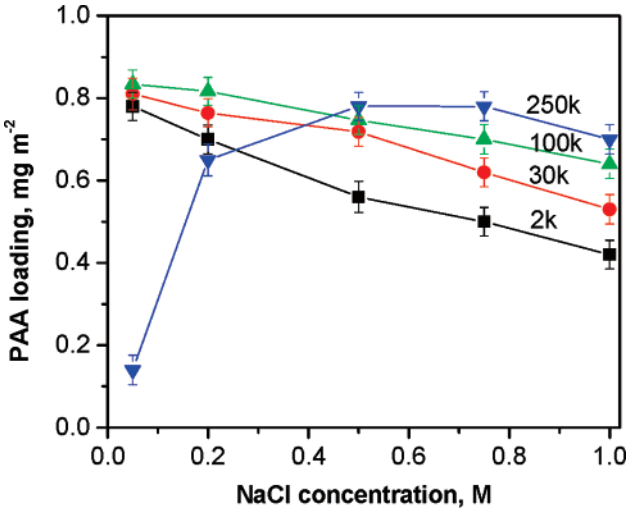

Figure 6. Influence of NaCl concentration on PAA loading for the various PAA molecular weights (adsorption time, 24 h; PAA/silica mass ratio, 1; nanoporous particles, S_{11}; and pH, 4.5).

be explained as follows. At 0.05 M NaCl, the extended conformation of PAA-250k restricts adsorption to mainly the surface of the particles, despite the relatively strong electrostatic attraction that exists between the PAA molecules and the nanopores at low salt concentrations because the diameter of PAA-250k (17.2 ± 0.2 nm; DLS data not shown) is significantly larger than the pore diameter for the S_{11} particles (10.6 nm). However, as the NaCl concentration is increased to 0.2 M, PAA-250k infiltration increases considerably due to increased screening of the polyelectrolyte charge by salt ions, which compacts the macromolecules (diameter, 10 ± 2.0 nm; DLS data not shown) and enables them to penetrate the pores of the S_{11} particles more efficiently. Above 0.5 M NaCl, the weakening electrostatic attraction between the PAA molecules and the nanopores outweighs any further reduction in the PAA-250k molecular size, and so the loading decreases with salt concentration.

Microscopy Characterization of PAA Infiltration in Nanopores. To verify that the PAA molecules infiltrate the nanopores, polymeric replicas were prepared and examined via TEM. The polymeric replicas were obtained by (i) cross-linking (via amide linkages) the loaded PAA molecules using ethylenediamine in the presence of EDC[7b,c] and (ii) dissolving the MS particles using diluted HF. PAA-30k, PAA-100k, and PAA-250k were used for these experiments because the effects of pore size and ionic strength on PAA infiltration are more pronounced at higher PAA molecular weights.

Figure 7a,b shows TEM images of the replicas prepared by infiltrating PAA-250k (with 0.5 M NaCl) and PAA-100k (with 0.05 M NaCl), respectively, in the $S_{3,28}$ particles. These replicas retain the spherical shape of the original $S_{3,28}$ particles and show no signs of collapse upon drying. This is in contrast to what is typically observed for hollow capsules prepared via the sequential assembly of polymers on the surface of nonporous template particles.[30] The diameter of the replicas ranges from 0.8 to 1.2 μm, representing a size reduction of ca. 60% relative to the original $S_{3,28}$ particles, which is comparable to that observed for nanoporous PAA/PAH spheres prepared by sequentially coating sacrificial $S_{3,28}$ particles.[7a,c] There is no obvious aggregation of the replicas. Figure 7c is a TEM image of the replicas prepared from the $S_{3,28}$ particles using PAA-250k in the presence of 0.05 M NaCl. The collapsed capsular structure of these replicas suggests that the extended conformation of PAA-250k at low salt limits adsorption to primarily the particle surface. Similar results were obtained using the S_{11} particles. That is, the morphology of the S_{11} particles can be replicated by infiltrating PAA-250k in the presence of 0.5 M NaCl (Figure 7d) and PAA-100k in the presence of 0.05 M NaCl (Figure 7e), but a hollow structure is produced when PAA-250k in the presence of 0.05 M NaCl is used (Figure 7f). In the case of the S_6 particles, replicas can be prepared using PAA-30k in the presence of 0.5 M NaCl, but not PAA-100k in the presence of 0.5 M NaCl. In the case of the S_4 particles, a hollow structure is produced when PAA-30k in the presence of 0.5 M NaCl is used.

The structures of the various replicas shown in Figure 7 are in good agreement with both the loading data and the R_h data obtained by TGA and DLS, respectively. Given that the preparation of stable polymeric replicas relies on the adsorption of polymer within the nanopores (which account for the majority of the surface areas of the templates), the successful formation of replicas in this study (Figure 7) verifies that the PAA molecules infiltrate the nanopores under the conditions employed.

To examine the distribution of PAA within the MS particles and the adsorption properties following PAA infiltration, DOX (a cationic anti-cancer drug) was bound electrostatically to the loaded PAA molecules, and the fluorescence resulting from the polymer−drug complex was observed through CLSM.[31] The $S_{3,28}$ particles were employed in these experiments due to the

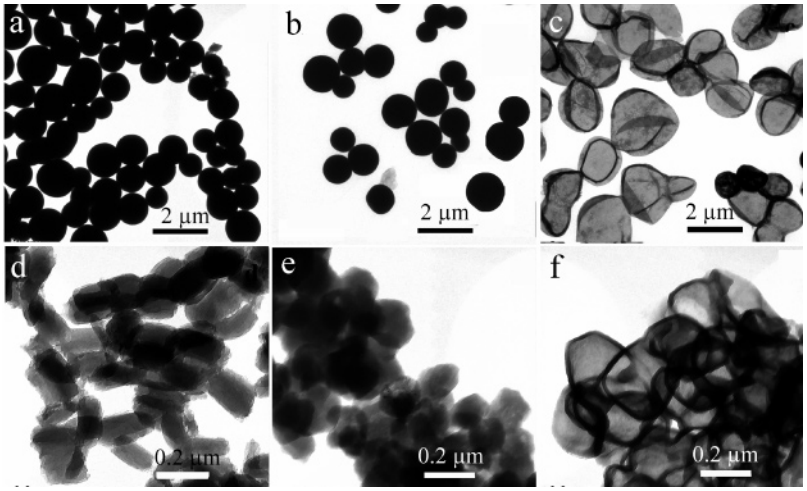

Figure 7. TEM images of the stable polymeric replicas obtained by cross-linking the loaded PAA molecules and then dissolving the MS particles. The particles used are (a−c) $S_{3,28}$ and (d−f) S_{11}. PAA molecular weights and NaCl concentrations used are (a and d) 250 000 g mol^{-1}, 0.5 M; (b and e) 100 000 g mol^{-1}, 0.05 M; and (c and f) 250 000 g mol^{-1}, 0.05 M. For panels a−f: adsorption time, 24 h; PAA/silica mass ratio, 1; and pH, 4.5.

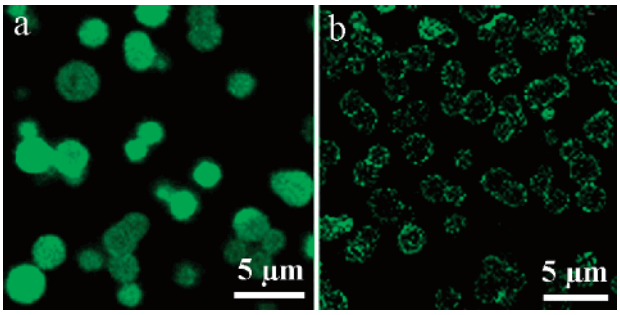

Figure 8. CLSM images of $S_{3,28}$ particles after infiltration of PAA-250k using (a) 0.5 M NaCl (adsorption time, 24 h; PAA/silica mass ratio, 1; and pH, 4.5) or (b) 0.05 M NaCl (adsorption time, 24 h; PAA/silica mass ratio, 1; and pH, 4.5), followed by incubation in DOX and washing. Fluorescence observed arises from DOX.

relatively large size (particle diameter, 2−3 μm) and regular spherical morphology of the particles. Additionally, the different regions of the particles (i.e., core vs outer surface) can be readily distinguished under the microscope. Figure 8 shows CLSM images of the $S_{3,28}$ particles after infiltration of PAA-250k, followed by incubation in DOX (0.04 mg mL^{-1}) for 5 min and thorough washing with Milli-Q water. When PAA-250k is infiltrated in the presence of 0.5 M NaCl (Figure 8a), uniform fluorescence is observed across the particle cross-sections due to the homogeneous distribution of DOX (and hence the effective infiltration of PAA) within the particles. When PAA-250k is infiltrated in the presence of 0.05 M NaCl (Figure 8b), however, significantly weaker (ca. 7 times) ring fluorescence is observed, indicating that relatively small amounts of DOX (and hence PAA) are present, mainly on the surface of the particles. These results are consistent with both the TGA data obtained (Figure 6) and the structures of the replicas prepared (Figure 7). Importantly, these results demonstrate that polymer-infiltrated MS particles exhibit a potential for loading materials, the amount/distribution of which can be tuned by simply adjusting the conditions (e.g., ionic strength) during the polymer infiltration step.

Conclusion

We have examined the use of a weak polyelectrolyte, PAA, to probe the accessibility of nanopores in amine-functionalized MS particles to macromolecules. It was found that the particle pore size and the PAA molecular weight significantly influence the loading process. The particles with larger nanopores (>10 nm) are capable of adsorbing a broader range of PAA molecular weights. In addition, it was observed that the adsorption conditions play an important role in PAA infiltration. The pH and ionic strength of the PAA solution govern the conformation of the macromolecules and hence the ability of the macromolecules to infiltrate the nanopores. For example, as the pH increases, the PAA charge density increases, and the polymer chains adopt a more rigid, linear conformation, resulting in a lower loading. In the presence of salt, the degree of loading depends upon a balance between screening of the polyelectrolyte charge (which promotes infiltration) and screening of the particle surface charge. It was also shown that the PAA-infiltrated MS particles possess excellent loading capacity for DOX. This approach is highly versatile in that the type and concentration of functional groups used to modify the nanopores can be readily controlled through the choice of polymer and adsorption conditions, respectively. Such polymer-modified nanoporous particles could find applications in biosensing, biocatalysis, drug delivery, and protein separation.

Acknowledgment. This work was supported by the Australian Research Council under the Discovery Project and Federation Fellowship Schemes and by the Victorian State Government under the STI Initiative. We acknowledge the Particulate Fluids Processing Centre for infrastructure support. Almar Postma is thanked for the SEM measurements.

References and Notes

(1) Kresge, C. T.; Leonowicz, M. E.; Roth, W. J.; Vartuli, J. C.; Beck, J. S. *Nature* **1992**, *359*, 710.
(2) For a detailed review, see: Hartmann, M. *Chem. Mater.* **2005**, *17*, 4577.
(3) (a) Han, Y. J.; Kim, J. M.; Stucky, G. D. *Chem. Mater.* **2000**, *12*, 2068. (b) Liu, Z.; Sakamoto, Y.; Ohsuna, T.; Hiraga, K.; Terasaki, O.; Ko, C. H.; Shin, H. J.; Ryoo, R. *Angew. Chem., Int. Ed.* **2000**, *39*, 3107.
(4) (a) Tian, B.; Liu, X.; Yang, H.; Xie, S.; Yu, C.; Tu, B.; Zhao, D. *Adv. Mater.* **2003**, *15*, 1370. (b) Dong, A.; Ren, N.; Tang, Y.; Wang, Y.; Zhang, Y.; Hua, W.; Gao, Z. *J. Am. Chem. Soc.* **2003**, *125*, 4976.
(5) (a) Ryoo, R.; Joo, S. H.; Jun, S. *J. Phys. Chem. B* **1999**, *103*, 7743. (b) Ryoo, R.; Joo, S. H.; Kruk, M.; Jaroniec, M. *Adv. Mater.* **2001**, *13*, 677.
(6) (a) Göltner, C. G.; Henke, S.; Weissenberger, M. C.; Antonietti, M. *Angew. Chem., Int. Ed.* **1998**, *37*, 613. (b) Kageyama, K.; Tamazawa, J.-I.; Aida, A. *Science* **1999**, *285*, 2113. (c) Kim, J. Y.; Yoon, S. B.; Kooli, F.; Yu, J. *J. Mater. Chem.* **2001**, *11*, 2912.

(7) (a) Wang, Y.; Yu, A.; Caruso, F. *Angew. Chem., Int. Ed.* **2005**, *44*, 2888. (b) Wang, Y.; Caruso, F. *Adv. Mater.* **2006**, *18*, 795. (c) Wang, Y.; Caruso, F. *Chem. Mater.* **2006**, *18*, 4089.
(8) (a) Xu, X.; Tian, B.; Kong, J.; Zhang, S.; Liu, B.; Zhao, D. *Adv. Mater.* **2003**, *15*, 1932. (b) Dai, Z.; Liu, S.; Ju, H.; Chen, H. *Biosens. Bioelectron.* **2004**, *19*, 861.
(9) (a) Diaz, J. F.; Balkus, K. F., Jr. *J. Mol. Catal. B: Enzym.* **1996**, *2*, 115. (b) Deere, J.; Magner, E.; Wall, J. G.; Hodnett, B. K. *Chem. Commun.* **2001**, 465. (c) Gomez, J. M.; Deere, J.; Goradia, D.; Cooney, J.; Magner, E.; Hodnett, B. K. *Catal. Lett.* **2003**, *88*, 183. (d) Wang, Y.; Caruso, F. *Chem. Commun.* **2004**, 1528.
(10) Radu, D. R.; Lai, C. Y.; Jeftinija, K.; Rowe, E. W.; Jeftinija, S.; Lin, V. S. Y. *J. Am. Chem. Soc.* **2004**, *126*, 13216.
(11) Han, Y. J.; Stucky, G. D.; Butler, A. *J. Am. Chem. Soc.* **1999**, *121*, 9897.
(12) (a) Washmon-Kriel, L.; Jimenez, V. L.; Balkus, K. J., Jr. *J. Mol. Catal. B: Enzym.* **2000**, *10*, 453. (b) Vinu, A.; Murugesan, V.; Tangermann, O.; Hartmann, M. *Chem. Mater.* **2004**, *16*, 3056.
(13) (a) de Gennes, P. G. *J. Chem. Phys.* **1971**, *55*, 572. (b) Doi, M.; Edwards, S. F. *J. Chem. Soc., Faraday Trans. 2* **1978**, *74*, 1789.
(14) Lumpkin, O.; Levene, S. D.; Zimm, B. H. *Phys. Rev. A* **1989**, *39*, 6557.
(15) Gabashvili, I. S.; Grosberg, A. Y. *J. Biomol. Struct. Dyn.* **1992**, *9*, 911.
(16) Smith, D. E.; Perkins, T. T.; Chu, S. *Phys. Rev. Lett.* **1995**, *75*, 4146.
(17) Reith, D.; Müller, B.; Müller-Plathe, F.; Wiegand, S. *J. Chem. Phys.* **2002**, *116*, 9100.
(18) Zhao, D.; Huo, Q.; Feng, J.; Chmelka, B. F.; Stucky, G. D. *J. Am. Chem. Soc.* **1998**, *120*, 6024.
(19) Zhang, H.; Sun, J.; Ma, D.; Bao, X.; Klein-Hoffmann, A.; Weinberg, G.; Su, D.; Schlögl, R. *J. Am. Chem. Soc.* **2004**, *126*, 7440.
(20) Schulz-Ekloff, G.; Rathouský, J.; Zukal, A. *Int. J. Inorg. Mater.* **1999**, *1*, 97.
(21) Walcarius, A.; Etienne, M.; Lebeau, B. *Chem. Mater.* **2003**, *15*, 2161.
(22) TGA data are presented in terms of the mass of PAA adsorbed per unit area of silica. Alternatively, the TGA data could be presented in terms of the number of PAA molecules adsorbed per unit area of silica. For example, the loadings of PAA-2k, PAA-8k, PAA-30k, PAA-100k, and PAA-250k in the 6 nm pores may be expressed as 0.54, 0.48, 0.40, 0.35, and 0.30 mg m^{-2}, respectively (Figure 3b) or 2×10^{17}, 4×10^{16}, 8×10^{15}, 2×10^{15}, and 5×10^{14} molecules m^{-2}, respectively.
(23) (a) Wang, Y.; Caruso, F. *Chem. Mater.* **2005**, *17*, 953. (b) Yu, A.; Wang, Y.; Barlow, B.; Caruso, F. *Adv. Mater.* **2005**, *17*, 1737.
(24) Choi, J.; Rubner, M. F. *Macromolecules* **2005**, *38*, 116.
(25) Burke, S. E.; Barrett, C. J. *Langmuir* **2003**, *19*, 3297.
(26) Hammouda, B.; Horkay, F.; Becker, M. L. *Macromolecules* **2005**, *38*, 2019.
(27) (a) Steitz, R.; Leiner, V.; Siebrecht, R.; Klitzing, R. *Colloids Surf., A* **2000**, *163*, 63. (b) Steitz, R.; Jaeger, W.; Klitzing, R. *Langmuir* **2001**, *17*, 4471. (c) Dubas, S. T.; Schlenoff, J. B. *Macromolecules* **2001**, *34*, 3736. (d) Ren, K.; Wang, Y.; Ji, J.; Lin, Q.; Shen, J. *Colloids Surf., B* **2005**, *46*, 63.
(28) Shiratori, S. S.; Rubner, M. F. *Macromolecules* **2000**, *33*, 4213.
(29) Schweins, R.; Hollmann, J.; Huber, K. *Polymer* **2003**, *44*, 7131.
(30) Donath, E.; Sukhorukov, G. B.; Caruso, F.; Davis, S. A.; Möhwald, H. *Angew. Chem., Int. Ed.* **1998**, *37*, 2201.
(31) Kitaeva, M. V.; Melik-Nubarov, N. S.; Menger, F. M.; Yaroslavov, A. A. *Langmuir* **2004**, *20*, 6575.

MA071125S